Journal of *Marine Science and Engineering*

MDPI

Article

Magnetic Plug Sensor with Bridge Nonlinear Correction Circuit for Oil Condition Monitoring of Marine Machinery

Yuwei Zhang [1], Jiaju Hong [1], Haotian Shi [1], Yucai Xie [1], Hongpeng Zhang [1,*], Shuyao Zhang [2], Wei Li [1] and Haiquan Chen [1]

[1] School of Marine Engineering College, Dalian Maritime University, Dalian 116026, China
[2] School of Navigation College, Dalian Maritime University, Dalian 116026, China
* Correspondence: zhppeter@dlmu.edu.cn

Abstract: Diesel engines in marine power systems often work in extreme environments. Oil monitoring technology can guarantee the operational safety of diesel engines. In this paper, a magnetic plug sensor for oil debris monitoring is proposed to improve sensitivity and accuracy. Through finite element analysis, absolute deviation is reduced by optimizing the sensor structure. A bridge nonlinear correction circuit is designed to make sensitivity consistent over the entire scale range, which can facilitate calibration and data processing. In order to reduce noise and amplify the signal effectively, a signal post-processing circuit is adopted as well, which consists of a first stage filter circuit, a second stage filter, an active filter module, and an instrumentation amplifier. Therefore, this magnetic plug sensor exhibits better sensitivity and accuracy. Furthermore, a void test and a dynamic test are carried out to investigate its performance. There is a linear relationship between the voltage and the particle mass for the sensor with a bridge nonlinear correction circuit. The results illustrate a minimum of 0.033 mg iron debris with a 1.647 signal-to-noise ratio. Additionally, it can capture and detect 47 μm particles with a debris capture rate of over 90%, which allows it to excel in early fault diagnosis as well.

Keywords: magnetic plug sensor; bridge nonlinear correction circuit; high sensitivity; high accuracy

Citation: Zhang, Y.; Hong, J.; Shi, H.; Xie, Y.; Zhang, H.; Zhang, S.; Li, W.; Chen, H. Magnetic Plug Sensor with Bridge Nonlinear Correction Circuit for Oil Condition Monitoring of Marine Machinery. *J. Mar. Sci. Eng.* **2022**, *10*, 1883. https://doi.org/10.3390/jmse10121883

Academic Editor: Mohamed Benbouzid

Received: 21 October 2022
Accepted: 17 November 2022
Published: 3 December 2022

1. Introduction

Diesel engines in marine power systems often work under extreme environments such as high temperature, overpressure, high humidity, and heavy load [1]. Ensuring safe operation of the diesel engine is a prerequisite to ensure the reliable operation of ships. By analyzing the information on wear debris in the oil tank of the diesel engine lubrication system, the wear condition of a diesel engine can be acquired [2]. Almost 80% of all metal parts are made of steel. It is of high practical value to install online sensors in the oil tank to monitor iron particles, so that the diesel engine can be maintained intelligently [3]. This would help to ensure the safe operation of vessels [4].

Online monitoring sensors based on different principles include optical/imaging wear particle detectors [5], electrical wear particle detectors [6], and magnetic plug sensors. Optical/imaging wear particle detectors can grasp the most comprehensive information about the particles [7]. However, they are rarely used in oil tanks because of their large size [8], together with their large deviation when the detector is in the oil with low light transmission [9]. Electrical wear particle detectors are usually installed in the pipe of the lubrication system [10], since their accuracy is easily affected by the flow rate of oil [11]. While in contrast, magnetic plug sensors can be installed in the tank. Additionally, their accuracy is not affected by oil light transmission and flow rate [12].

Magnetic plug sensors mainly consist of a detection coil and a permanent magnet, and can continuously capture and detect wear particles. These features make them very suitable for online monitoring. They have long been used in the wear detection area,

and are discussed in depth by researchers again in recent years through the concept of online monitoring. Bogue et al. [13] designed a magnetoresistive sensor, which had eight electrodes evenly distributed on both ends of the magnet. Debris was captured on the side of the magnet conducting those electrodes and outputting a signal, which is related to wear condition. Muthuvel et al. [14] innovatively used a coil as one pole of a capacitor and a permanent magnet as the other pole of a capacitor to monitor wear debris. Cao et al. [15] placed a planar inductive coil under the capture area of permanent magnet. The above magnetic plug sensors are not sensitive enough for early fault diagnosis of mechanical equipment. Muthuvel et al. [16] placed a planar inductive coil over the capture area of permanent magnet, which shortened the distance between the coil and particles. As a result, it improved sensitivity. Shi et al. [17] improved sensitivity by combing an inductive bridge circuit and a capacitive bridge circuit to analyze the information on iron particles. However, it may have had a low particle capture rate because of the small detection area. In addition, its nonlinear relationship between the voltage and debris mass has not been analyzed and corrected. There is still a defect in sensitivity and accuracy.

In this paper, a magnetic plug sensor with high sensitivity and high accuracy is proposed. The sensor has a detection unit and a reference unit with the same structure. The unit is an inductor coil with a built-in permanent magnet. The ring permanent magnet is adopted to reduce the absolute deviation of this sensor. A bridge nonlinear correction circuit measures the change of impedance caused by iron particles making sensitivity consistent over the entire scale range. At the same time, a signal post-processing circuit is utilized to improve signal-to-noise ratio. Thus, the proposed sensor has high sensitivity and high accuracy, which is important for preventive maintenance, servicing, and preventing catastrophic failures.

2. Magnetic Plug Sensor Design

A schematic of the magnetic plug sensor structure is shown in Figure 1. The permanent magnet captures wear debris in the detection unit. Another unit with the same structure is set as a reference unit. They are the bridge arms of the bridge nonlinear correction circuit. Their inductive coils have a 12 mm inner diameter (D_1), a 20 mm outer diameter (D_2), and a 3 mm height (H_2). The wire diameter of the coil is 0.2 mm and the number of turns is 114. The magnets have a 12 mm diameter (D_1) and a 2 mm height (H_1). Because of the skin effect, there is a magnetic flux density difference value between the inner side and the center of the coil. The absolute deviation caused by the different particle capture positions may need to be taken into account as well.

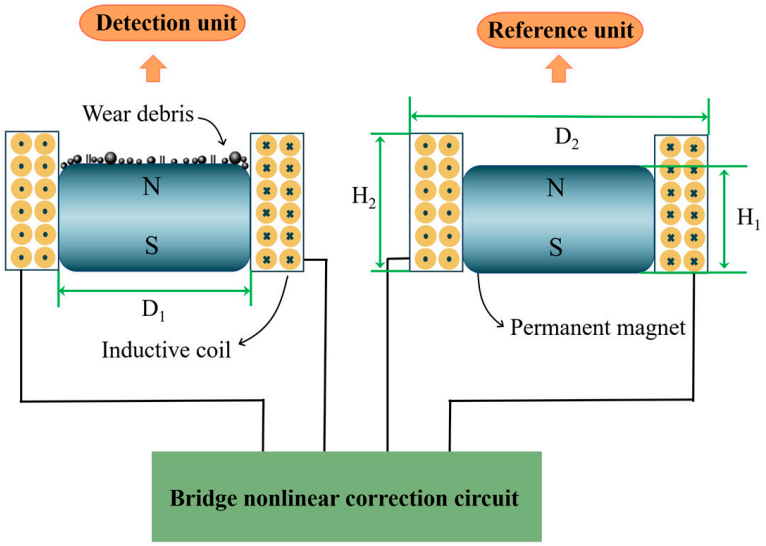

Figure 1. Structure diagram of magnetic plug sensor.

2.1. Strutural Optimization

To reduce the absolute deviation, a ring permanent magnet is utilized in the sensor. The effects of the cylindrical permanent magnet and ring permanent magnet on the detection unit are compared by finite element analysis. The finite element analysis is performed using COMSOL Multiphysics. The modeling process is as follows: selecting the 3D spatial dimension and AC/DC module, setting magnetic field without current and magnetic field physical fields, selecting the frequency domain study, adding materials, dividing the mesh, performing coil geometry analysis, and parametric scanning.

2.1.1. Details of Finite Element Analysis

Firstly, the geometric models are built. A geometric model of the detection unit with a ring permanent magnet is shown in Figure 2a. The coordinate origin is located on the upper surface center of the ring magnet. The magnet has a 12 mm outer diameter, 8 mm inner diameter, and is 2 mm high. A geometric model with a cylindrical permanent magnet is shown in Figure 3a. This magnet has a 12 mm outer diameter and is 2 mm high. Coils have a 12 mm inner diameter, 20 mm outer diameter, and are 3 mm high. The diameter of the spherical particle is 1 mm. The spherical air domain has a 30 mm diameter.

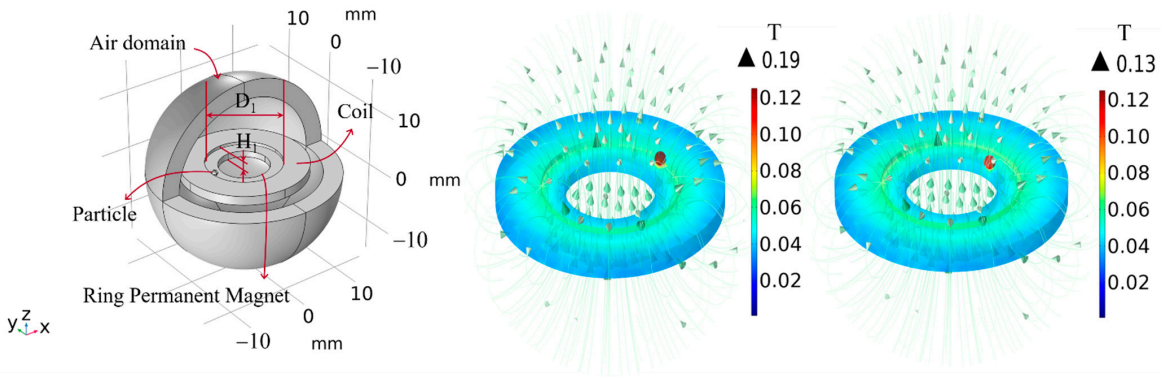

(**a**) (**b**) (**c**)

Figure 2. Electromagnetic simulation of detection unit with a ring permanent magnet: (**a**) 3D model of the detection unit with a particle; (**b**) Magnetic flux density mode distribution of the particle at position (5.5 mm, 0 mm, 0.5 mm); (**c**) Magnetic flux density mode distribution of the particle at position (4.125 mm, 0 mm, 0.5 mm).

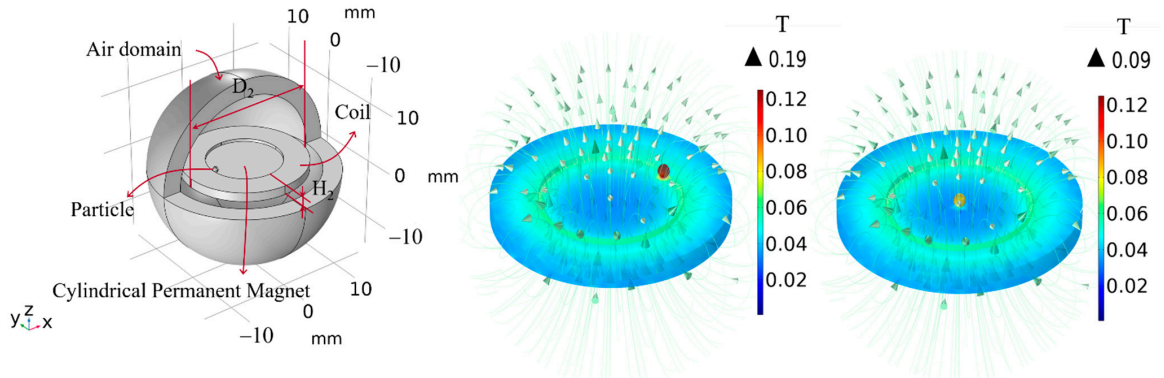

(**a**) (**b**) (**c**)

Figure 3. Electromagnetic simulation of detection unit with a cylindrical permanent magnet: (**a**) 3D model of the detection unit with a particle; (**b**) Magnetic flux density mode distribution of the particle at position (5.5 mm, 0 mm, 0.5 mm); (**c**) Magnetic flux density mode distribution of the particle at position (0 mm, 0 mm, 0.5 mm).

The material components air, copper, and iron are added to the air domain, the coil, and the particle, respectively, from the material library in the software. The material of the ring permanent magnet is NdFeB. It needs to be made by adding empty material and setting the material properties: relative permeability 1.03, relative permittivity 1, and electrical conductivity 1.8×10^6 S/m.

In a magnetic field without current, "magnetic flux conservation 2" is created. The constitutive relation chooses magnetization. The magnetization direction of the PM is the *Z*-axis direction, and the value is 750,000 A/m. In the magnetic field, "coil 1" is created. The wire type is chosen to have a uniform multi-turn, the number of turns is 114, the diameter of the round wire is 0.2 mm, and the excitation voltage is 10 V. The surface of air domain is set as an infinite elementary domain.

In the meshing, the particle, coil, and permanent magnet are selected as free tetrahedral meshes and chosen to be more refined. For the air domain, a free tetrahedral mesh is chosen and coarsened.

The study is performed by setting up the parametric scan, the coil geometry analysis, and the frequency domain analysis in turn. For parametric scanning, particle position is set as (−5.5 + *l* mm, 0 mm, 1.5 mm). The value "*l*" is the distance a particle moves from its position (−5.5 mm, 0 mm, 1.5 mm) along the *X*-axis direction, it ranges from 0 mm to 11 mm and its step size is 1.375 mm. Finally, we have completed the setup and start calculating.

2.1.2. Results of Finite Element Analysis

After completing the calculation, COMSOL Multiphysics generates the magnetic flux density modes of the particle at different locations of the sensing unit directly as shown in Figures 2b,c and 3b,c. Afterwards, the global calculation can be added to the derived values in the result for obtaining the inductance of the coil when the particle is in different positions, as shown in Figure 4.

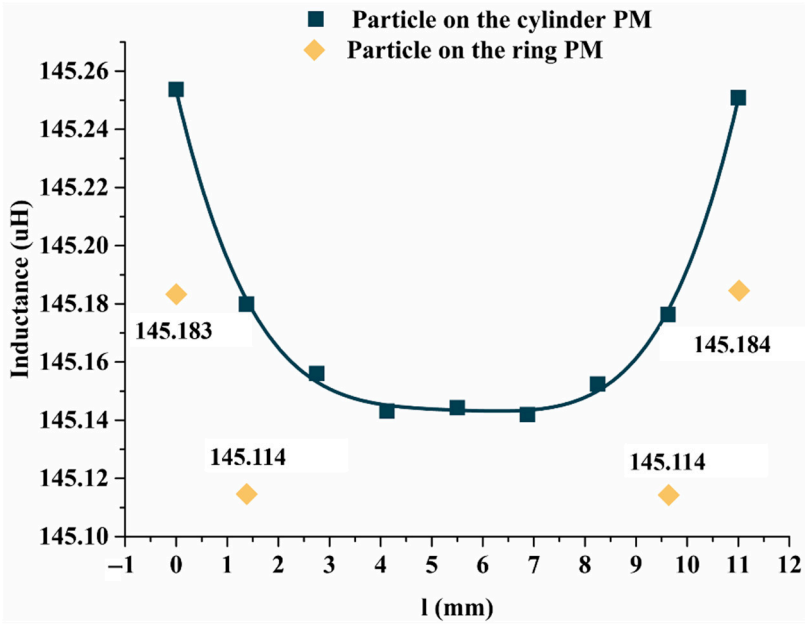

Figure 4. Effect of particle position on coil inductance.

As shown in Figures 2b and 3b, an iron particle is magnetized to the maximum extent at the position (5.5 mm, 0 mm, 0.5 mm) where the magnetic flux density modulus is 0.19 T. Different magnet structures have equivalent magnetization ability in the same position. Additionally, in Figure 2c the particle is magnetized at the position (4.125 mm, 0 mm, 0.5 mm) where the magnetic flux density modulus is 0.13 T. As shown in Figure 3c, a particle magnetized at position (0 mm, 0 mm, 0.5 mm) reaches 0.09 T. Thus, comparing

with that using a ring permanent magnet, the sensor using a cylindrical permanent magnet has a larger difference value of magnetic flux density modulus.

As shown in Figure 4, whatever detection unit adopts the cylindrical magnet or the ring magnet, the closer a particle is to the inside of the coil, the larger inductance of the coil output. However, their "value 1" and "absolute deviation" are different, as shown in Table 1. Consequently, comparing the detection unit with the ring permanent magnet, "value 1" is larger in the detection unit with the cylindrical permanent magnet. A high "value 1" can contribute to the sensitivity. Comparing the detection unit with the cylindrical permanent magnet, the "absolute deviation" is smaller in the detection unit with the ring permanent magnet. Low "absolute deviation" can contribute to the accuracy of the sensor. Therefore, the ring type does not have a positive influence on sensitivity but has an advantage in accuracy. Deliberately, sensitivity can be improved by circuits. The detection unit with a ring permanent magnet is chosen to increase the accuracy.

Table 1. Effects of detection unit with different structure type of permanent magnet.

	Cylindrical Type	Ring Type
value 1 (μH)	0.232	0.098
absolute deviation (μH)	0.073	0.035

"value 1" is the inductance change of the coil between with and without the particle on the inner surface of the coil. This "absolute deviation" is the difference between the inductance value of the particle at (5.5 mm, 0 mm, 0.5 mm) position and the average value.

2.2. Bridge Nonlinear Correction Circuit

A bridge circuit as a comparative measurement instrument has high sensitivity. In a complex and harsh environment, it also has a certain anti-interference effect and is used in signal detection, usually. However, its inherent nonlinearity makes sensitivity inconsistent over the entire scale range, which complicates data analysis and processing. To facilitate calibration and data processing, the output voltage of the detection system needs to be linearized. Sensor as a leading edge of the detection system directly affects the precision. In Figure 5a,b, Z_1 is the detection unit and Z_2 is the reference unit. u_s is the excitation voltage and u_0 is the output voltage. Iron particles are magnetized by the detection unit, which causes a change in inductance value ΔZ. The output voltages of a bridge circuit and a bridge nonlinear correction circuit are analyzed separately below.

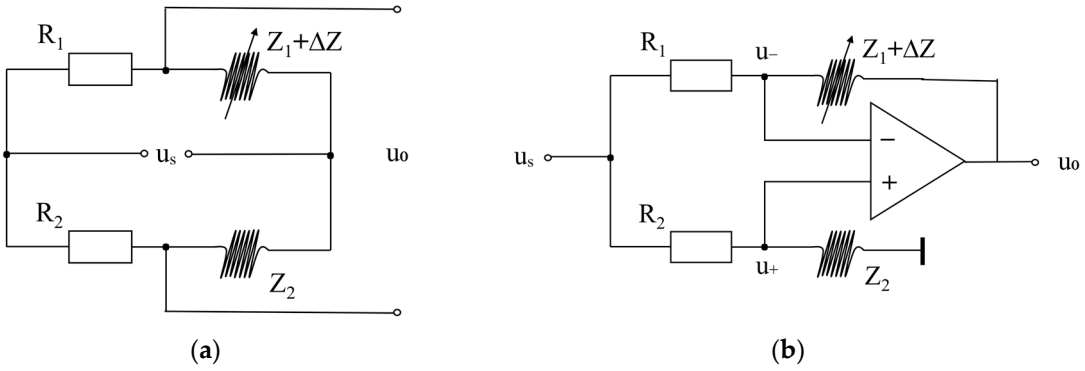

Figure 5. Circuit Simplification: (**a**) Bridge circuit; (**b**) Bridge nonlinear correction circuit.

As shown in Figure 5a, according to Kirchhoff laws, the output voltage of the bridge circuit is

$$u_0 = \left(\frac{Z_1 + \Delta Z}{R_1 + Z_1 + \Delta Z} - \frac{Z_2}{R_2 + Z_2}\right)u_s \quad (1)$$

When the bridge is balanced $R_1 = R_2 = R$, $Z_1 = Z_2 = Z$, its output voltage is

$$u_0 = \frac{R}{R+Z}(1 - \frac{R+Z}{R+Z+\Delta Z})u_s \quad (2)$$

Therefore, the bridge circuit is nonlinear whether the bridge is balanced or unbalanced. As shown in Figure 5b, the output voltage of the bridge nonlinear correction circuit is

$$u_+ = \frac{Z_2}{R_2+Z_2}u_s \quad (3)$$

$$u_- = \frac{R_1}{R_1+Z_1+\Delta Z}u_0 + \frac{Z_1+\Delta Z}{R_1+Z_1+\Delta Z}u_s \quad (4)$$

$$u_0 = (\frac{Z_2R_1 - Z_1R_2}{R_1(R_2+Z_2)} - \frac{R_2\Delta Z}{R_1(R_2+Z_2)})u_s \quad (5)$$

When the bridge is balanced $R_1 = R_2 = R$, $Z_1 = Z_2 = Z$, its output voltage is

$$u_0 = -\frac{\Delta Z}{R+Z}u_s \quad (6)$$

Thus, the bridge nonlinear correction circuit is linear both in balance or unbalanced state.

3. Detection System and Circuit

As shown in Figure 6, the detection system consists of a detection unit, a reference unit, a signal processing circuit, a DAQ card (NI USB 6211, National Instruments, Austin, TX, USA), a DC power supply (Agilent E3631A, Agilent, Santa Clara, CA, USA), a wave generator (KEYSIGHT 33600A Series, KEYSIGHT, PA, USA), and a computer with a LabVIEW program. The detection unit and reference unit are placed in the oil tank separately. The wave generator provides a 10 V, 4.2 MHz excitation signal. The computer stores and displays signals.

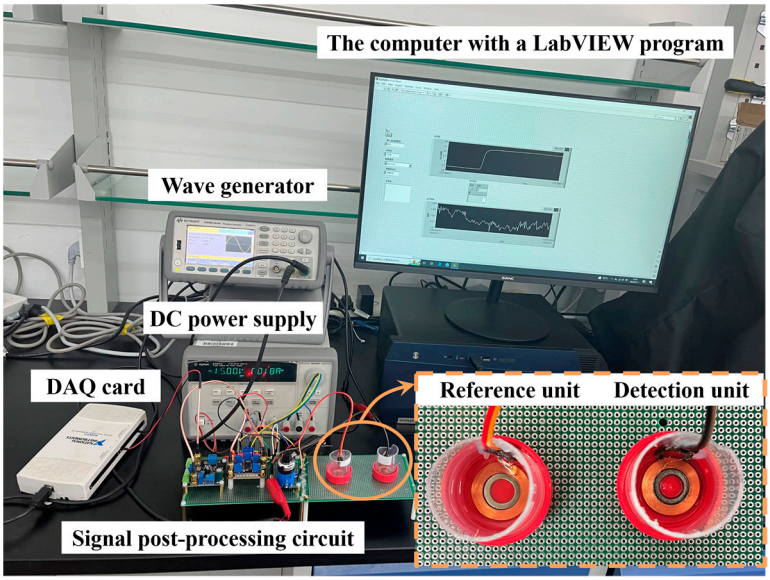

Figure 6. Photo of the detection system.

The signal processing circuit is shown in Figure 7. Iron particles captured by the detection unit cause an impedance change ΔZ, which is processed by a bridge nonlinear correction circuit outputting u_0. Then u_0 is filtered and amplified. In this paper, the excitation frequency is 4.2 MHz. The output voltage u_0 needs to pass through a first stage filter circuit with a low pass cutoff frequency set to 100 kHz and a second stage filter circuit

with a low pass cutoff frequency set to 10 kHz. These two filters are both voltage-controlled power supply type second order low-pass filters and both use the AD826, a dual, high speed voltage feedback op-amp with a 50 MHz bandwidth. Then an active filter module (UAF42) can be used. It is a general-purpose active filter that can be configured for low-pass, high-pass and band-pass filters, with an inverting amplifier and two integrators. In this paper, the UAF42 is configured for use as a low-pass filter whose input frequency range is DC—1 MHz, and has a low-pass cutoff frequency of 5 kHz. Finally, the signal is amplified with the instrumentation amplifier (AD623), a weak signal amplifier that can amplify input voltages from 100 uV to 1 Vpp by a factor of 1 to 1000, to obtain a voltage signal with a high signal-to-noise ratio.

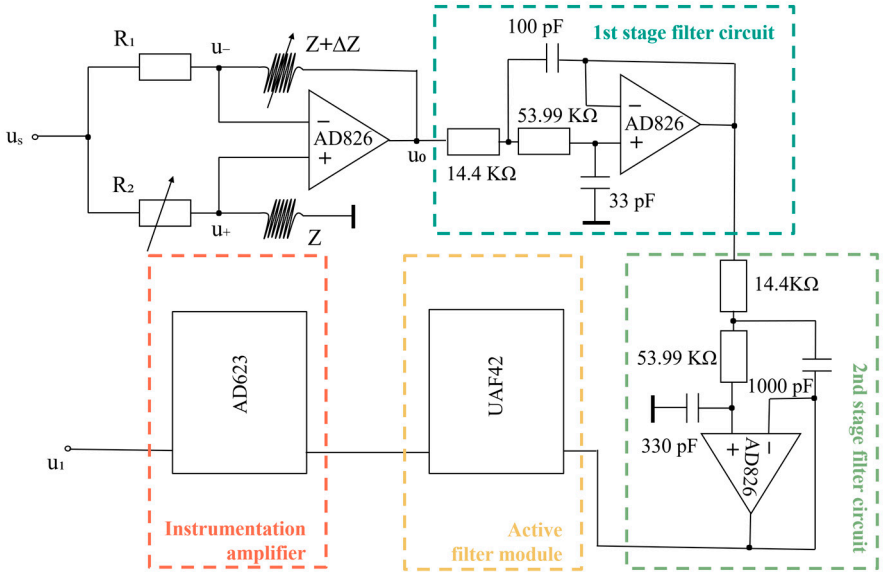

Figure 7. Schematic diagram of signal processing circuit.

4. Experiment and Discussion

In the experiment, due to the distribution of wires and craftsmanship of components, it is impossible to guarantee that $R_1 = R_2 = R$, $Z_1 = Z_2 = Z$. This means that when $\Delta Z = 0$, there is a certain base voltage that will be amplified in the signal post-processing circuit causing the useful signal to be drowned out. By replacing R_2 with a precision adjustable resistor and adjusting the frequency of excitation voltage, the base voltage can be minimized. At the same time, the frequency of excitation voltage also affects the sensitivity of the sensor. Considering the base voltage and sensor sensitivity, the precision adjustable resistor R_2, and excitation voltage frequency are adjusted. Finally, the excitation voltage frequency is determined to be 4.2 MHz.

4.1. Void Test

To investigate the sensitivity and accuracy of the sensor, a void test is performed. It examines the effect of different masses of iron particles on the sensor in an oil-free experimental environment. Spherical iron particles with different sizes are used as experimental samples to characterize different masses of particles (S_1, S_2, S_3, S_4, S_5, S_6, S_7). The relationship between particle size and mass parameters is shown in Table 2. Particles are glued onto a 0.47 mm diameter nylon wire separately. Capture duration and times are controlled by the wire. A particle is detected for more than 5 s 6 times.

Figure 8 shows the response to different masses. The noise is 0.044 V, and the signal-to-noise ratio reaches 1.647 for 0.033 mg debris. Because the testing range is ±5 V and the data acquisition card is 16 bits, the resolution is 152.6 uV. In addition, the relationship between particle mass and the voltage signal is basically linear, as shown in Figure 9. Consequently, the proposed sensor has high sensitivity and accuracy.

Table 2. Comparison table of particle size and mass.

Oil Sample	Diameter (μm)	Mass (mg)
S_1	200	0.033
S_2	300	0.111
S_3	400	0.263
S_4	500	0.514
S_5	600	0.888
S_6	700	1.411
S_7	800	2.106

Each oil sample has a spherical iron particle.

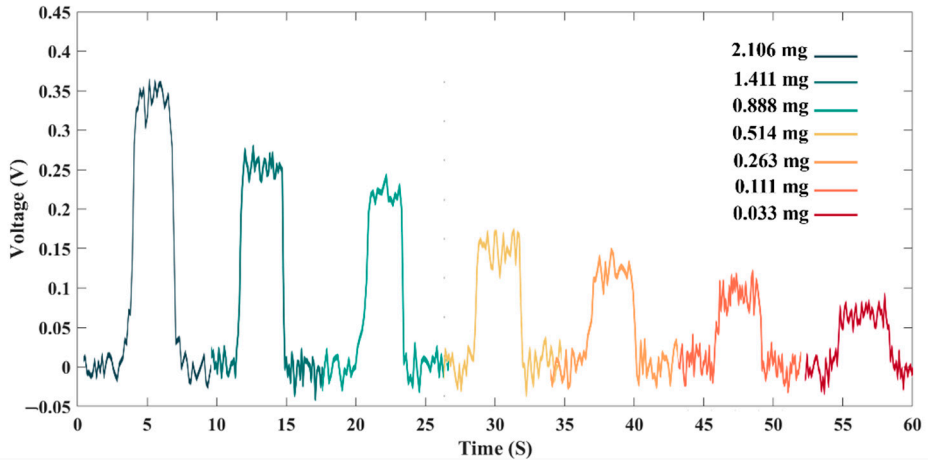

Figure 8. Response of the sensor to different masses of debris.

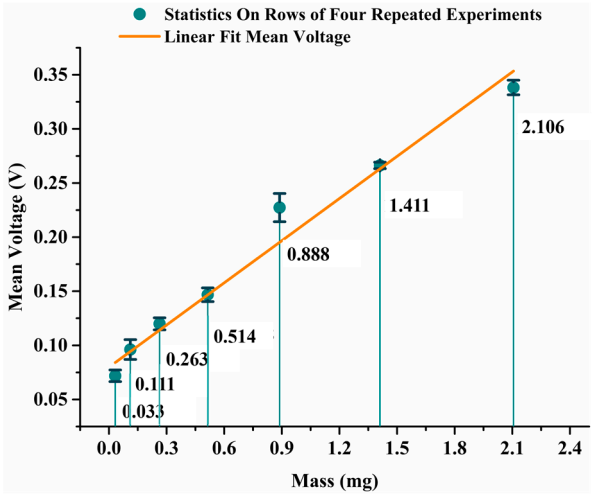

Figure 9. Output voltages of the sensor. Each error bar is derived from the data of six replicate experiments.

4.2. Dynamic Test

In the dynamic test, the effect of particle mass and size on the output voltage and particle capture rate in an oil tank is explored. Firstly, oil samples are configured with different mass concentrations. In a test tube, 5 mg 47 μm particles are weighed by a precision balance. A volume of 15 mL of hydraulic oil is poured into the test tube. It is well shaken by a high-speed centrifuge for 15 min to obtain oil sample L_1, which is 333 PPM. In another test tube, 5 mg 100 μm debris is weighed. A volume of 15 mL of hydraulic oil is poured into this test tube. It is fully shaken using a high-speed centrifuge for 15 min, then 15 mL oil is added and it is fully shaken again. After that, half of the sample is extracted to

a new test tube, then 15 mL oil is added and it is fully shaken again to obtain oil sample L_2, which is 83 PPM.

After commissioning the detection system, an investigation started. Firstly, 1 mL oil sample L_1 is added to the oil tank. When the signal stabilizes, 1 mL oil sample L_2 is added to it secondly. As shown in Figure 10, the 333 PPM oil simple can produce a voltage change of 1.19749 V and the 86 PPM oil sample can produce a voltage change of 0.51163 V. Notably, oil sample L_1 consists of 47 µm particles, which are smaller than the 100 µm particles in oil sample L_2. Oil sample L_1 can lead to a larger voltage change compared with the other one. Therefore, signal change is related to the mass of debris and not the particle size.

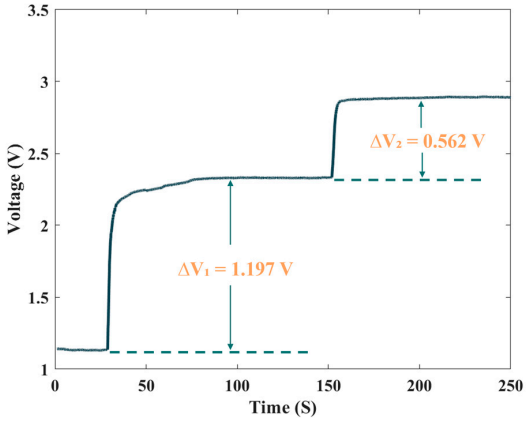

Figure 10. Concentration signal graph.

In addition, in Figure 10, after 1 mL L_1 is poured into the oil tank, voltage stabilization is taken at about 50 s. However, the effect of 1 mL L_2 on voltage stabilization takes about 10 s. It is implied that it takes a longer time for 47 µm particles to be captured and detected, because of their smaller gravity and magnetization. Thus, particle size has a minor influence on the voltage stabilization time but won't affect the magnitude of signal.

Experiments demonstrate that the magnetic plug sensor can capture and detect iron particles smaller than 50 µm. They are present in the early stages of mechanical wear. Therefore, this sensor can achieve early fault warnings.

To observe the capture rate, oil sample L_3 is configured, which come from a mixture of oil sample L_1 and oil sample L_2 after completing the test. Then, three drop oils are taken from fully oscillating oil sample L_1, oil sample L_2, and oil sample L_3, respectively. Each of them is placed on a glass carrier sheet. As shown in Figure 11a, many 47 µm iron particles are presented in L_1. They are flocculent particles visible to the naked eye. As shown in Figure 11b, a small amount of 100 µm iron particles are visible to the naked eye. They exist independently of each other. As shown in Figure 11c, there are few iron particles in oil sample L_3. So, it is concluded that the debris capture rate is over 90% with this sensor.

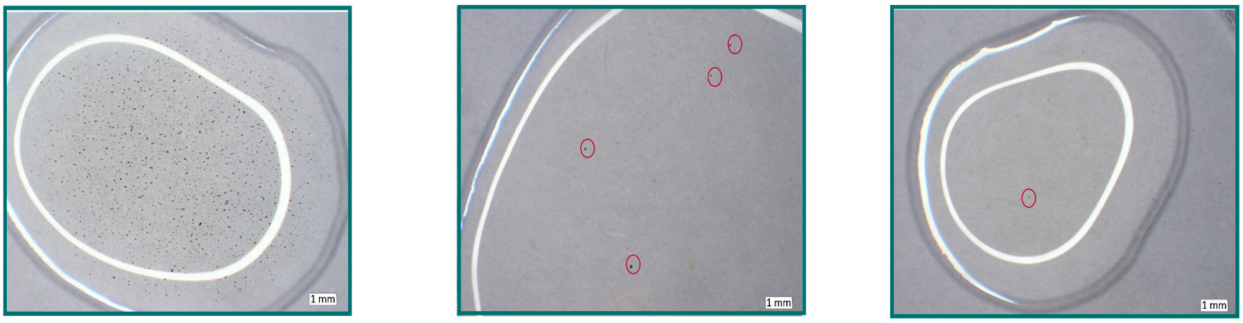

(**a**) (**b**) (**c**)

Figure 11. Oil samples: (**a**) Oil sample L_1 needs to be tested, 47 µm, 333 PPM; (**b**) Oil sample L_2 needs to be tested, 100 µm, 83 PPM; (**c**) Oil sample L_3 after testing.

4.3. Discussion

Overall, we found that the magnetic plug sensor has high sensitivity and accuracy after optimizing its permanent magnet structure and incorporating a bridge nonlinear correction circuit and a signal post-processing circuit. In Figure 9, the sensor has a linear characteristic curve for a given measurement range with a good fit. This will help to simplify the calibration of the sensor in use and is important for improving accuracy. However, previous magnetic plug sensors have not paid attention to this point. At the same time, researchers have not studied and addressed the impact of particle position on the accuracy of magnetic plug sensors. We reduce this impact by investigating and utilizing the ring permanent magnets and improve sensor accuracy further. In addition, most researchers are currently able to detect particles in amounts as little as 10 mg in oil [12,14,16], and one is able to respond to a single particle of 200 um [17]. This sensor is capable of responding to 2.5 mg of particles in oil and can detect a particle of 200 um. Therefore, we can conclude from Table 3 that the magnetic plug sensor proposed in this paper has high accuracy and high sensitivity, which is important for predicting and diagnosing diesel engine faults. However, this sensor is in the design phase, and its sensing unit, reference unit, and circuit are not yet packaged as a whole. In the process of packaging, considering the installation environment and shielding technique can further improve the stability of the sensor.

Table 3. Comparison of key technical parameters with other magnetic plug sensors.

Author	Dynamic Test	Void Test	Linearity	Particle Location Impact	Ref.
Harkemance, E.	10 mg	-	-	-	[12]
Itomi, S.	20 mg	-	-	-	[13]
Muthuvel, P.	10 mg	-	-	-	[14]
Cao, Y.P	100 mg	-	-	-	[15]
Muthuvel, P.	10 mg	-	-	-	[16]
Shi, H.T.	-	200 um	N	Big	[17]
Our work	2.5 mg	200 um	Y	A little	

Reproduced from [12], with permission from Proceedings, 2018. Reproduced from [13], with permission from U.S. Patent, 2006. Reproduced from [14], with permission from IEEE Sens, 2018. Reproduced from [15], with permission from 2018 13th ICST, 2018. Reproduced from [16], with permission from 2019 13th ICST, 2019. Reproduced from [17], with permission from IEEE TIM, 2022.

5. Conclusions

This paper proposes a magnetic plug sensor for online wear monitoring high in sensitivity and accuracy. According to finite element analysis, the ring permanent magnet has a positive influence on the accuracy of the sensor. A bridge nonlinear correction circuit can correct the nonlinearity from the signal output principle, which will facilitate calibration and data processing. A signal post-processing circuit is adopted to further improve the signal-to-noise ratio of the sensor, which ultimately could identify a minimum of 0.03291 mg iron debris with a 1.647 signal-to-noise ratio. Moreover, this sensor can capture 47 μm iron particles in the oil tank and has a particle capture rate of over 90%. Thus, the proposed magnetic plug sensor based on a bridge nonlinear correction circuit not only has high sensitivity and accuracy, but also has superior performance in detecting tiny abrasive particles in the oil tank. It is important for preventive maintenance and preventing catastrophic failures in marine diesel engines.

Author Contributions: Conceptualization, Y.Z.; Data curation, Y.Z. and S.Z.; Formal analysis, Y.Z.; Funding acquisition, H.Z. and W.L.; Investigation, H.S. and H.Z.; Methodology, Y.Z., H.S. and Y.X.; Software, Y.Z.; Supervision, H.Z. and H.C.; Validation, Y.Z. and Y.X.; Writing—original draft, Y.Z. and J.H.; Writing—review and editing, Y.Z., J.H. and H.S. All authors have read and agreed to the published version of the manuscript.

Funding: This research was funded by Natural Science Foundation of China, grant number 51679022; Natural Science Foundation of China, grant number 52271303; Dalian Science Technology Innovation Fund, grant number 2019J12GX023; Liaoning Revitalization Talents Program, grant number XLYC2002074; Fundamental Research Funds for the Central Universities, grant number 3132022219; Fundamental Research Funds for the Central Universities, grant number 3132021501; Science and Technology Innovation Foundation of Dalian, grant number 2021JJ11CG004.

Institutional Review Board Statement: Not applicable.

Informed Consent Statement: Not applicable.

Data Availability Statement: Data is contained within the article.

Conflicts of Interest: The authors declare that we do not have any commercial or associative interest that represent a conflict of interest in connection with the work submitted.

References

1. Liang, X.H.; Zou, M.J.; Feng, Z.P. Dynamic modeling of gearbox faults: A review. *MSSP* **2018**, *98*, 852–876. [CrossRef]
2. Fan, B.; Li, B.; Feng, S.; Mao, J.; Xie, Y.B. Modeling and experimental investigations on the relationship between wear debris concentration and wear rate in lubrication systems. *Tribol. Int.* **2017**, *109*, 114–123. [CrossRef]
3. Sun, J.; Wang, L.; Li, J.; Li, F.; Li, J.; Lu, H. Online oil debris monitoring of rotating machinery: A detailed review of more than three decades. *MSSP* **2021**, *149*, 107341. [CrossRef]
4. Zhu, X.L.; Zhong, C.; Zhe, J. Lubricating oil conditioning sensors for online machine health monitoring—A review. *Tribol. Int.* **2017**, *109*, 473–484. [CrossRef]
5. Xi, W.; Wu, T.; Yan, K.; Yang, X.; Jiang, X.; Kwok, N. Restoration of online video ferrography images for out-of-focus degradations. *J. Image Video Process.* **2018**, *2018*, 31. [CrossRef]
6. Mehri, T.; Kemppinen, O.; David, G.; Lindqvist, H.; Tyynelä, J.; Nousiainen, T.; Rairoux, P.; Miffre, A. Investigating the size, shape and surface roughness dependence of polarization lidars with light-scattering computations on real mineral dust particles: Application to dust particles' external mixtures and dust mass concentration retrievals. *Atmos. Res.* **2018**, *203*, 44–61. [CrossRef]
7. Amann, S.; Witzleben, M.V.; Breuer, S. 3D-printable portable open-source platform for low-cost lens-less holographic cellular imaging. *Sci. Rep.* **2019**, *9*, 11260. [CrossRef] [PubMed]
8. Schoell, R.; Xi, L.; Zhao, Y.; Wu, X.; Yu, Z.; Kenesei, P.; Almer, J.; Shayer, Z.; Kaoumi, D. In situ synchrotron X-ray tomography of 304 stainless steels undergoing chlorine-induced stress corrosion cracking. *Corros. Sci.* **2020**, *170*, 108687. [CrossRef]
9. Jin, Z.; Zhang, F.Q. Analysis of spatial sensitivity based on electrostatic monitoring technique in oil-lubricated system. *Open Access Libr. J.* **2018**, *5*, 1–13. [CrossRef]
10. Qian, M.; Ren, Y.J.; Zhao, G.F.; Feng, Z. Ultrasensitive inductive debris sensor with a two-stage auto asymmetry compensation circuit. *IEEE TIE* **2021**, *68*, 8885–8893.
11. Muthuvel, P.; George, B.; Ramadass, G.A. A Highly Sensitive In-Line Oil Wear Debris Sensor Based on Passive Wireless LC Sensing. *IEEE Sens. J.* **2021**, *21*, 6888–6896. [CrossRef]
12. Harkemance, E.; Berten, O.; Hendrick, P. Analysis and Testing of Debris Monitoring Sensors for Aircraft Lubrication Systems. *Proceedings* **2018**, *2*, 416.
13. Itomi, S. Oil Condition Sensor. U.S. Patent US7151383 [P], 26 September 2006.
14. Muthuvel, P.; George, B.; Ramadass, G.A. Magnetic-Capacitive Wear Debris Sensor Plug for Condition Monitoring of Hydraulic Systems. *IEEE Sens. J.* **2018**, *18*, 9120–9127. [CrossRef]
15. Cao, Y.; Liu, R.; Du, J.; Yu, F.; Yang, Q.; He, Y.; Li, S. Gas Turbine Bearing Wear Monitoring Method Based on Magnetic Plug Inductance Sensor. In Proceedings of the 2018 13th ICST, Oslo, Norway, 11–15 June 2018.
16. Muthuvel, P.; George, B.; Ramadass, G.A. A planar inductive based oil debris sensor plug. In Proceedings of the 2019 13th ICST, NSW, Australia, 2–4 December 2019.
17. Shi, H.T.; Bai, C.Z.; Xie, Y.C.; Li, W.; Zhang, H.; Liu, Y.; Zheng, Y.; Zhang, S.; Zhang, Y.; Lu, H.; et al. Capacitive–Inductive Magnetic Plug Sensor with High Adaptability for Online Debris Monitoring. *IEEE TIM* **2022**, *71*, 1–8. [CrossRef]